Journal of Magnetic Resonance 289 (2018) 122–131

Contents lists available at ScienceDirect

Journal of Magnetic Resonance

journal homepage: www.elsevier.com/locate/jmr

Verdazyl-ribose: A new radical for solid-state dynamic nuclear polarization at high magnetic field

Kent R. Thurber [a,*], Thanh-Ngoc Le [b], Victor Changcoco [b], David J.R. Brook [b]

[a] Laboratory of Chemical Physics, National Institute of Diabetes and Digestive and Kidney Diseases, National Institutes of Health, Bethesda, MD 20892-0520, United States
[b] Department of Chemistry, San José State University, One Washington Square, San José, CA 95192, United States

ARTICLE INFO

Article history:
Received 30 August 2017
Revised 20 February 2018
Accepted 21 February 2018
Available online 1 March 2018

Keywords:
Verdazyl
Radical
Dynamic nuclear polarization
Cross-effect mechanism
Solid state NMR
Magic-angle spinning

ABSTRACT

Solid-state dynamic nuclear polarization (DNP) using the cross-effect relies on radical pairs whose electron spin resonance (ESR) frequencies differ by the nuclear magnetic resonance (NMR) frequency. We measure the DNP provided by a new water-soluble verdazyl radical, verdazyl-ribose, under both magic-angle spinning (MAS) and static sample conditions at 9.4 T, and compare it to a nitroxide radical, 4-hydroxy-TEMPO. We find that verdazyl-ribose is an effective radical for cross-effect DNP, with the best relative results for a non-spinning sample. Under non-spinning conditions, verdazyl-ribose provides roughly 2× larger ^{13}C cross-polarized (CP) NMR signal than the nitroxide, with similar polarization buildup times, at both 29 K and 76 K. With MAS at 7 kHz and 1.5 W microwave power, the verdazyl-ribose does not provide as much DNP as the nitroxide, with the verdazyl providing less NMR signal and a longer polarization buildup time. When the microwave power is decreased to 30 mW with 5 kHz MAS, the two types of radical are comparable, with the verdazyl-doped sample having a larger NMR signal which compensates for its longer polarization buildup time. We also present electron spin relaxation measurements at Q-band (1.2 T) and ESR lineshapes at 1.2 and 9.4 T. Most notably, the verdazyl radical has a longer T_{1e} than the nitroxide (9.9 ms and 1.3 ms, respectively, at 50 K and 1.2 T). The verdazyl electron spin lineshape is significantly affected by the hyperfine coupling to four ^{14}N nuclei, even at 9.4 T. We also describe 3000-spin calculations to illustrate the DNP potential of possible radical pairs: verdazyl-verdazyl, verdazyl-nitroxide, or nitroxide-nitroxide pairs. These calculations suggest that the verdazyl radical at 9.4 T has a narrower linewidth than optimal for cross-effect DNP using verdazyl-verdazyl pairs. Because of the hyperfine coupling contribution to the electron spin linewidth, this implies that DNP using the verdazyl radical would improve at lower magnetic field. Another conclusion from the calculations is that a verdazyl-nitroxide bi-radical would be expected to be slightly better for cross-effect DNP than the nitroxide-nitroxide bi-radicals commonly used now, assuming the same spin-spin coupling constants.

Published by Elsevier Inc.

1. Introduction

Dynamic nuclear polarization (DNP) transfers spin polarization from unpaired electron spins to nuclear spins. This can increase the nuclear spin polarization, which improves the sensitivity of nuclear magnetic resonance (NMR) measurements. Crucial to DNP are radical molecules which can be doped into the sample to provide the unpaired electron spins. The radicals used for DNP need to satisfy several different criteria. Most importantly, the radicals need to be efficient at polarizing the nuclear spins. There are several different mechanisms for DNP including the cross-effect [1,2], the solid-effect [3,4], thermal mixing [5–7], and the Overhauser effect [8,9], which have different requirements for the radicals, especially for the electron spin resonance (ESR) linewidth. In our case of DNP of ^{1}H nuclei at high magnetic field (9.4 T) with moderate strength microwave irradiation of the solid-state sample, the cross-effect is the dominant mechanism. Cross-effect DNP needs two electron spins whose ESR frequencies differ by the NMR frequency [2,10]. Currently, nitroxide radicals are primarily used for cross-effect DNP of ^{1}H [11,12], because the large g-anisotropy of the nitroxides allows two nitroxides with different radical orientations to have a frequency difference equal to the ^{1}H frequency. Although nitroxide pairs are effective for cross-effect DNP of ^{1}H, however they are not as efficient as they could be because only a fraction of the possible nitroxide pair orientations will have a frequency difference match-

* Corresponding author at: National Institutes of Health, Building 5, Room 116, Bethesda, MD 20892-0520, United States.
E-mail address: thurberk@niddk.nih.gov (K.R. Thurber).

https://doi.org/10.1016/j.jmr.2018.02.016
1090-7807/Published by Elsevier Inc.

ing the NMR frequency [10]. Thus, it is useful to investigate the DNP properties of other radicals.

In addition to efficient nuclear polarization, for our application of DNP to biomolecules [13,14], we generally want the radicals to be stable and soluble in water/glycerol mixtures, so the radicals can be easily mixed into a solution with the sample of interest. Then, the water/glycerol mixture is frozen, providing a glassy matrix for the radicals and biomolecules during DNP measurements at low temperatures.

This paper reports high field solid-state DNP experiments testing a recently synthesized water-soluble verdazyl radical molecule, verdazyl-ribose (Fig. 1) [15]. Verdazyl radicals were discovered in 1963 [16,17], and can be very stable in the solid-state and in solution. Under some conditions, verdazyl-ribose is more stable than nitroxide radicals. For example, ascorbic acid rapidly reacts with nitroxide radicals, but does not react significantly with the verdazyl [15]. Verdazyl radicals have been used successfully for liquid-state DNP at relatively low magnetic field (up to 1.4 T) [18,19], but to our knowledge have not been previously used for high magnetic field DNP. In this article, we measure solid-state DNP using the verdazyl-ribose radical at 9.4 T, both with and without MAS, and compare it to the nitroxide radical, 4-hydroxy-TEMPO. The verdazyl-ribose radical does provide significant cross-effect DNP. With a non-spinning sample, the sample with verdazyl gives roughly 2× larger ^{13}C CP NMR signal than the sample with nitroxide, and similar polarization buildup times. With 7 kHz MAS and 1.5 W microwave power at 30 K, the sample with verdazyl provides only 60% of the signal of the nitroxide sample, and also has a longer polarization buildup time. When the microwave power is reduced to 30 mW at 5.2 kHz MAS, the DNP from the two radicals is comparable, with the larger NMR signal from the verdazyl sample compensating for its longer polarization buildup time.

We also present solid-state ESR spectra of the verdazyl radical at 1.2 T (Q-band) and 9.4 T at 50 K, and the temperature dependence of ESR T_{1e} and T_m relaxation measurements at 1.2 T. The ESR spectra show that the electron spin has a nearly axial g-tensor and strong anisotropic hyperfine couplings to all four ^{14}N nuclei in the ring of the radical molecule. Even at 9.4 T, these hyperfine couplings have a significant effect on the ESR lineshape. Quantum chemistry calculations suggest that the principal axis perpendicular to the plane of the verdazyl ring has the smallest g-value and the largest ^{14}N hyperfine coupling. From the relaxation measurements, the most notable result is that the verdazyl has a significantly longer T_{1e} than the nitroxide at 1.2 T and 50 K.

Also presented here are calculations of spin systems to estimate the cross-effect DNP efficiency of hypothetical bi-radicals, either verdazyl-verdazyl, nitroxide-nitroxide, or verdazyl-nitroxide pairs.

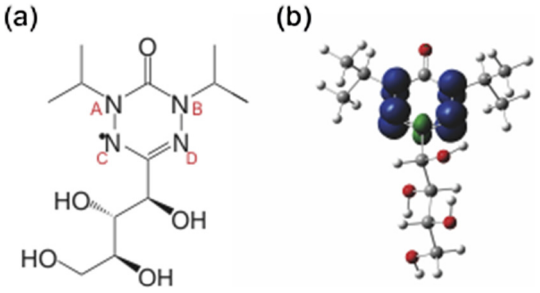

Fig. 1. (a) Structure of verdazyl-ribose. The four nitrogen atoms are labelled for reference in Table 3 and the text. (b) Electron spin density surface shown in blue (+) and green (−) on top of the molecular geometry from a quantum chemistry calculation. (For interpretation of the references to colour in this figure legend, the reader is referred to the web version of this article.)

The polarization dynamics of 1000 three-spin systems (two electron and one nuclear spins) is simulated using the Landau-Zener equation [20,21]. These calculations show that the ESR spectrum of this verdazyl radical is only barely wide enough for pairs of verdazyl radicals to meet the cross-effect frequency matching condition for ^{1}H nuclei at 9.4 T. This suggests that the verdazyl radical would be more efficient for DNP at lower magnetic field, because the field-independent hyperfine couplings would give the radical a larger ESR linewidth relative to the NMR frequency. The calculations also suggest that a hypothetical verdazyl-nitroxide bi-radical should be slightly better than a nitroxide-nitroxide bi-radical, if both bi-radicals have the same spin-spin couplings.

2. Experimental methods

The NMR experiments used the home-built ultra-low-temperature DNP-MAS NMR probe described previously [22] and were performed at 9.39 T (400.9 MHz and 100.8 MHz ^{1}H and ^{13}C NMR frequencies) using a Bruker Avance III NMR spectrometer console. For experiments with 30 mW of microwaves, the microwave source was a diode source from Virginia Diodes, Inc. mounted with the quasi-optical interferometer system previously described [23]. For experiments with 1.5 W of microwaves, the microwave source was an extended interaction oscillator (EIO) from Communications & Power Industries, which transmits its microwaves through a corrugated waveguide to the quasi-optical interferometer system [24]. The 45 μl NMR samples contained 40 mM of radicals, either verdazyl-ribose or 4-hydroxy-TEMPO, and 150 mM ^{15}N,$^{13}C_3$-L-alanine in partially protonated glycerol/water (60/30/10 volume% d_8-glycerol/D_2O/H_2O). The radical concentration is determined by measuring the optical absorption [15,25]. For the verdazyl radical, the optical absorption at the 382 nm peak in the glycerol/water solvent was 1100 cm^{-1} M^{-1}. Sample temperatures were determined from measurements of the spin-lattice relaxation of ^{79}Br in KBr contained in a glass capsule placed in the MAS rotor along with the sample [26].

For CP ^{13}C measurements, an 800 μs CP contact time and 40 kHz ^{13}C radio-frequency field strength were used, with one dummy scan to establish a steady state before NMR signal acquisition. In all ^{13}C NMR experiments, 75 kHz proton decoupling fields with two-pulse phase modulation [27] were applied during detection of free-induction decay (FID) signals. The ^{1}H nuclear polarization buildup times, τ_{DNP}, were measured by recovery from saturation of the ^{13}C CP signals, with the microwaves on. The recovery time from saturation for ^{13}C CP NMR was also measured with the microwaves off (^{1}H T_{1n}) at 31 K with MAS for the verdazyl dopant sample, and the time was not significantly different from the polarization buildup time with the microwaves on.

^{13}C CP NMR signals and DNP enhancements in Table 1 are calculated from the integrals of all alanine ^{13}C lines (CO, Cα, and Cβ signals) for measurements with MAS. Without MAS, the entire aliphatic region was integrated, thus including the alanine Cα and Cβ signals, and glycerol natural abundance ^{13}C signals. The NMR signal measurements were taken with repetition delays equal to twice the polarization buildup times. Measurement uncertainties are listed in Table 1, dominated by the uncertainty in absolute signal size, estimated at ~20% from multiple measurements on some samples.

1.2 T (Q-band) ESR measurements used a Bruker E-580 spectrometer and a model ER5107D2 probe. The Q-band ESR samples were 0.1 mM concentration of verdazyl or nitroxide in 60/40 volume% d_8-glycerol/D_2O. The 1.2 T ESR spectrum of Fig. 4 was taken by integrating the full echo from a $\pi/2$-τ_m-π-τ_m-echo pulse sequence, with a 512 ns π pulse and 5 μs τ_m. The microwave frequency was 33.94465 GHz for the verdazyl Q-band spectrum at

Table 1
Summary of DNP measurements with MAS for verdazyl-ribose and 4-hydroxy-TEMPO nitroxide dopants. The DNP enhancement (ε) is calculated as the ratio of the ^{13}C CP NMR signal integral with and without the microwaves. The overall DNP efficiency (Σ) is calculated as the ^{13}C CP NMR signal integral with the microwaves on, divided by the square root of the polarization buildup time, τ_{DNP}.

Microwave power	Dopant	Temperature (±2; K)	^{13}C signal, microwaves on (±20%; arb. units)	ε (±5%)	τ_{DNP} (±15%; s)	Σ (±20%)	MAS frequency (kHz)
1.5 W	Verdazyl	31	294	31	16.3	73	6.7
		85	64.9	25	7.45	24	6.9
		105	9.8	3.5	2.7	6.0	6.9
		150	2.4	1.7	1.3	2.1	7.0
	Nitroxide	30	506	81	10.1	159	7.0
		97	24.1	11	4.8	11.0	7.0
		160	2.7	1.4	2.1	1.9	7.0
30 mW	Verdazyl	22	237	14	21.1	51.6	5.2
		27	140	11	17.2	33.7	5.2
		44	82.5	9.3	19.6	18.6	5.4
		75	24.5	6.35	11.3	7.3	5.2
		97	8.1	3.55	6.6	3.2	5.3
	Nitroxide	30	77	10	9.9	24.5	5.2
		95	6.1	2.4	6.8	2.3	5.2

50 K, and the magnetic field was calibrated by fitting the 50 K spectrum of 4-hydroxy-TEMPO (taken with microwave frequency 33.97312 GHz) to the values of Ref [28]. For the ESR relaxation measurements, the microwave frequency was tuned in the range between 33.89 and 33.95 GHz. The relaxation measurements were taken at the maximum of the ESR spectra with a 16 ns π pulse and full echo integral. The spin-lattice relaxation time, T_{1e}, measurement used a π-τ_1-π/2-τ_m-π-τ_m-echo pulse sequence, with 0.4 μs τ_m. The phase memory relaxation time, T_m, measurement varied the delay time, τ_m, between pulses in a π/2-τ_m-π-τ_m-echo pulse sequence. The 9.4 T ESR lineshape was taken as described previously, by stepping the frequency of the 30 mW microwave source for each data point [23]. For the 9.4 T ESR, a 10 μl sample of 10 mM verdazyl in 60/40 volume% d_8-glycerol/D_2O was contained in a Teflon cup and mounted in a static-sample, liquid He-cooled cryostat (Janis SuperTran).

3. Experimental results

3.1. Dynamic nuclear polarization (DNP)

Fig. 2 shows examples of the DNP enhancement with the verdazyl-ribose radical for ^{13}C CP spectra with and without MAS. The DNP results are summarized for experiments with MAS in Table 1, and without MAS in Table 2. The DNP enhancement, ε, is measured as the ratio of the ^{13}C CP signal integrals with microwaves on and off. But it is important to compare more than just the DNP enhancement because even the NMR signal with the microwaves off can be significantly affected by the radical dopant [29]. A second reason that the microwave-off alanine ^{13}C CP signals do not follow a 1/T Boltzmann temperature dependence is dynamics, especially methyl group rotation [30]. In addition, the polarization buildup time, τ_{DNP}, determines how many signal measurements can be taken in a fixed amount of time. Thus, because the signal-to-noise ratio increases as the square root of the number of signal measurements averaged together, the signal-to-noise ratio is proportional to $1/\sqrt{\tau_{DNP}}$. To include these factors, the overall efficiency of DNP, Σ, is calculated as the ^{13}C CP signal integral with the microwaves on, divided by $\sqrt{\tau_{DNP}}$. This DNP efficiency value, Σ, is proportional to the signal-to-noise measured with DNP in a fixed amount of time.

The 40 mM of verdazyl-ribose radical does provide significant DNP with enhancements as large as 74×. For comparison, we also measure the DNP from the same L-alanine solution doped with 4-hydroxy-TEMPO nitroxide, instead of verdazyl-ribose. Here, we are

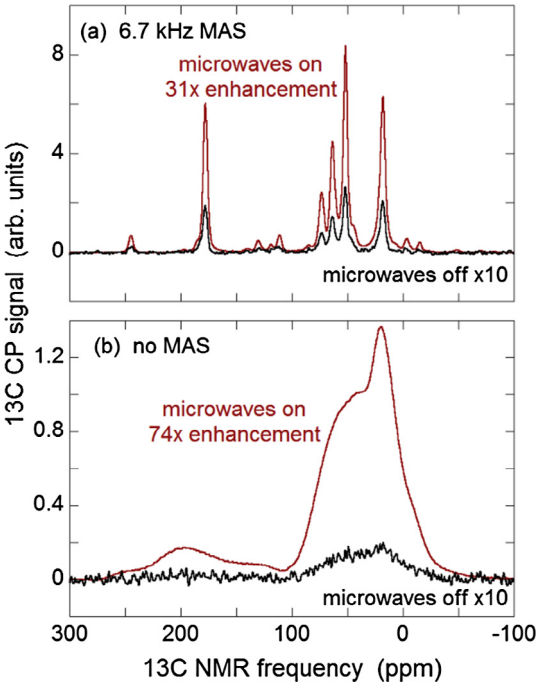

Fig. 2. (a) ^{13}C CP spectra of L-alanine in frozen glycerol/water showing DNP enhancement with MAS, and (b) without MAS, using 40 mM of verdazyl-ribose dopant and 1.5 W of microwaves at 263.8 GHz. Spectra shown in part (a) are 16 scans each at 31 K, and in part (b) are 4 scans each at 29 K.

comparing two single radical molecules, even though the best cross-effect DNP is achieved with bi- or tri-radical molecules [11,25]. If we compared the mono-radical verdazyl-ribose to bi- or tri-radical nitroxide molecules, it would be unclear what results to attribute to the radical characteristics, versus the difference between single and multi-radical molecules. To summarize the results, the verdazyl radical provides larger DNP enhancements than the nitroxide when the sample is not spinning. With MAS, 1.5 W microwave power, and low temperature (~30 K), the verdazyl has a smaller DNP efficiency, Σ, because of both smaller enhancement and longer polarization buildup time. If the microwave power is reduced, or the temperature is increased, the verdazyl DNP with MAS becomes comparable to the nitroxide.

To discuss the results in more detail, with 6.7–7 kHz MAS, 1.5 W microwave power, and at low temperatures, the verdazyl does not

Table 2
Summary of DNP measurements without MAS for verdazyl-ribose and 4-hydroxy-TEMPO nitroxide dopants.

Microwave power	Dopant	Temperature (±2; K)	^{13}C signal, microwaves on (±20%; arb. units)	ε (±5%)	τ_{DNP} (±15%; s)	Σ (±20%)
1.5 W	Verdazyl	29	855	74	31.9	151
		76	63.1	26	16.5	15.5
	Nitroxide	29	405	40	30.4	73.5
		80	26.8	10	14.9	6.9

provide as much nuclear polarization as the nitroxide. At 30–31 K, DNP enhancement for the verdazyl is only 40% of that for the nitroxide, and the NMR signal is only 60%. The fact that the NMR signal ratio is larger than the DNP enhancement ratio shows that the nuclear polarization loss from radical doping with MAS is smaller for the verdazyl than for the nitroxide. For the non-spinning measurements at 29 K, the ratios of DNP enhancement and absolute signals are within the error margin of each other. This indicates that the NMR signal losses from paramagnetism that do not depend on MAS are roughly equal for the two radicals. As a result, the extra signal loss for the nitroxide with MAS relative to the verdazyl can be attributed to MAS specific mechanisms, most likely the cross-effect DNP depolarization that can happen with MAS, even without microwaves [29]. So, the verdazyl has less MAS DNP depolarization without microwaves, but the MAS DNP enhancement with microwaves is also enough lower that the final absolute NMR signal is lower for the sample with verdazyl than for the sample with nitroxide. In addition, the polarization buildup time is slower, resulting in only roughly half the value of Σ. At higher temperature and 1.5 W microwave power, the two radicals have comparable Σ values. Specifically, comparing the result for the verdazyl at 150 K to the nitroxide at 160 K, the verdazyl sample has the shorter polarization buildup time, and the absolute signals differ by only ~10%. However, at these higher temperatures, the DNP enhancement is low for both radicals. When the microwave power is reduced to 30 mW, with 5.2–5.4 kHz MAS, at 27 K, the verdazyl sample has larger absolute NMR signal and longer polarization buildup time, which combine to provide DNP efficiency, Σ, comparable to the nitroxide sample. When the temperature is increased to 95–97 K, with 30 mW microwave power, and 5.2–5.3 kHz MAS, the verdazyl provides higher Σ, though the absolute enhancement is low for either radical in this case.

Without MAS, the verdazyl radical is better than the nitroxide. With 1.5 W microwave power, the NMR signal is roughly twice as large for the verdazyl-doped sample, both at 29 K and at 76/80 K. Because the polarization buildup times are similar, the verdazyl-doped sample also provides roughly twice the overall DNP efficiency, Σ.

Fig. 3(a) shows the dependence of the DNP enhancement of the verdazyl-doped sample on the microwave frequency with 30 mW of microwave power, with and without MAS. The microwave frequency dependence has significant asymmetry both with and without MAS. The maximum positive DNP enhancement is larger than the maximum negative DNP enhancement, and significant positive enhancements occur over a broader frequency region. This DNP asymmetry can be explained by the asymmetrical ESR lineshape, shown in Fig. 3(b), which is discussed in more detail below.

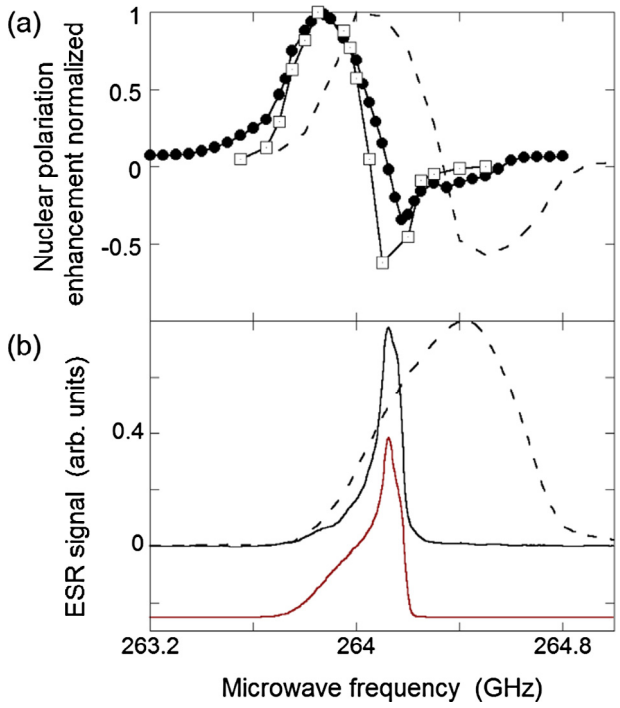

Fig. 3. (a) Nuclear polarization enhancement as a function of microwave frequency for 40 mM verdazyl-ribose and 30 mW microwave power, with 5.2 kHz MAS at 22 K (•) and without MAS at 29 K (□), normalized to maximum enhancement (14× with MAS, 59× without MAS). Dashed line shows normalized enhancement for nitroxide (40 mM 4-amino-TEMPO, 16 K, non-spinning) from Ref. [23]. (b) ESR lineshape at 9.4 T and 50 K (solid black line). Shown below in red is the fit from the parameters of Table 3. Dashed line is the nitroxide ESR lineshape from Ref. [23]. (For interpretation of the references to colour in this figure legend, the reader is referred to the web version of this article.)

3.2. Electron spin resonance

To investigate the properties of this verdazyl-ribose radical, we measured the electron spin lineshape and relaxation at 1.2 T (Q-band). Fig. 4 shows the pulsed ESR lineshape at 50 K in frozen glycerol/water solution. The most prominent features are 9 peaks & shoulders which can be attributed to the hyperfine coupling to the four ^{14}N nuclei in the ring of the radical. Since the ^{14}N nucleus is spin 1, the total ^{14}N spin varies in integer steps from −4 to +4, which can create 9 peaks and/or shoulders in the spectrum. Previous liquid state ESR at 0.3 T (X-band) shows that the electron spin has significant isotropic hyperfine couplings to all four ^{14}N nuclei [15]. The liquid state ESR also had smaller isotropic hyperfine couplings from three nearby ^{1}H nuclei. In our 1.2 T solid-state spectra, we do not see any additional resolved hyperfine couplings, suggesting that there are not any anisotropic ^{1}H hyperfine couplings large enough to be resolved in this spectrum.

We also measured the ESR lineshape at 9.4 T and 50 K, shown in Fig. 3(b). At 9.4 T, there is one large peak, with a tail extending to lower frequencies. This measurement has the advantage of being at the same magnetic field as the DNP measurements, and taken with the same microwave setup, so the ESR and DNP frequency dependence can be easily compared. However, we should note that the high radical concentration used (10 mM), and measurement of each point by changing the microwave frequency can cause some distortion of the ESR lineshape.

To gain a better understanding of the ESR lineshape, we ran quantum chemistry calculations using the Gaussian 09 program [31]. The main calculation used the B3LYP functional and implicit

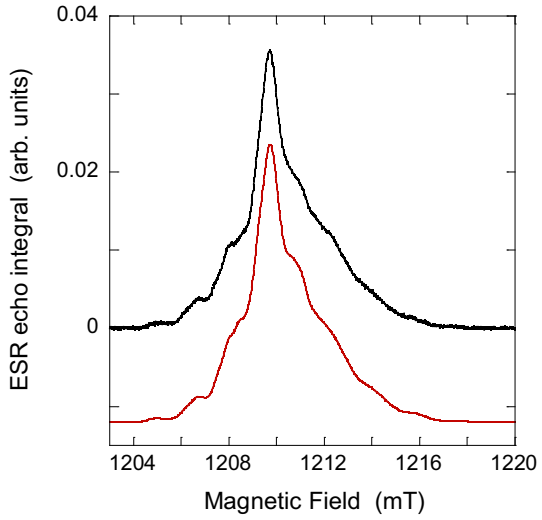

Fig. 4. Pulsed ESR lineshape of 0.1 mM verdazyl-ribose at 1.2 T (Q-band) and 50 K, with best fit shown below in red. Lineshape fitting parameters are given in Table 3. (For interpretation of the references to colour in this figure legend, the reader is referred to the web version of this article.)

water solvent, with the EPR-III basis set, which was designed for the calculation of hyperfine couplings [32]. As shown in Fig. 1(b), the unpaired electron spin is spread primarily over the four nitrogen atoms of the ring, with some negative spin density on the C atom at the base of the ring. The g-factor and hyperfine coupling results are shown in Table 3, and are consistent with previous calculations for other verdazyl radical molecules [33–35]. The calculation indicated a nearly axial g-tensor with the two principal axes in the plane of the ring having the two larger g values, while the third axis is perpendicular to the ring plane, with the smaller g value. The calculated ^{14}N hyperfine couplings are also nearly axial for all four nitrogens. There are large ^{14}N hyperfine couplings along the axis perpendicular to the ring plane, and very small couplings along the other two axes. By symmetry, the four nitrogens can be divided into two pairs. The two nitrogens bonded to the carbonyl carbon (labelled A & B in Fig. 1a) have almost equal primary hyperfine couplings, which are slightly smaller than the hyperfine couplings of the other two nitrogens. Comparing the principal axes of the g-tensor and the hyperfine couplings, the principal axes perpendicular to the ring plane are within one degree of each other. So, in summary, these calculations predict an axial tensor for both the g value and the ^{14}N hyperfine couplings, with the axis perpendicular to the ring plane having both a lower g value, and large ^{14}N hyperfine couplings. We also ran quantum chemistry calculations with other functionals and basis sets, without implicit water solvent. The results were qualitatively similar, and are shown in the Supplementary information Tables S1 & S2.

Fitting the 1.2 T ESR lineshape was done using the Easyspin program [36]. Based on trial fitting, and the quantum chemistry calculations, the number of variables in the fit was reduced by the following assumptions: (i) all of the ^{14}N hyperfine couplings have the same principal axes as the g-tensor, with the large hyperfine coupling aligned with the small g value; (ii) the two small principal hyperfine coupling values are equal; and (iii) the nitrogen atoms related by symmetry have the same hyperfine couplings. In addition, the width of the main peak of the 9.4 T ESR lineshape was used to estimate the difference between the two larger principal g values. The 1.2 T lineshape by itself could be consistent with the two larger g values being equal. Even with these simplifying assumptions, a good fit to the 1.2 T ESR lineshape is obtained (see Fig. 4). The best fit parameters found are listed in Table 3. Using the same parameters (except for a larger line broadening), also gives a reasonable fit to the lineshape at 9.4 T. The ESR lineshape at 9.4 T primarily reflects the axial g-tensor, but the ^{14}N hyperfine couplings are large enough to still influence the lineshape. If the lineshape was just determined by the axial g-tensor, it would have a much sharper low-frequency edge. Instead, because the largest hyperfine couplings are along the low g-value axis, the low-frequency edge of the ESR line is smeared out into a broad tail.

Fig. 5 shows ESR relaxation measurements at 1.2 T (Q-band). Most notably, the electron spin-lattice relaxation time, T_{1e}, of the verdazyl-ribose radical is over 7 times longer than the T_{1e} of 4-hydroxy-TEMPO at 50 K. T_{1e} of the verdazyl has a strong temperature dependence, with the T_{1e} time increasing by almost an order of magnitude from 50 to 25 K. In contrast, the phase memory relaxation time, T_m, has very little temperature dependence between 25 and 50 K, but is significantly shorter at 100 K. Compared to 4-hydroxy-TEMPO at 50 K, the phase memory relaxation of the verdazyl radical has a faster initial decay, while the later decay rate is very similar. The cause of the fast initial echo decay is not clear, perhaps it could be caused by some clustering of verdazyl radicals [37,38], or perhaps by the hyperfine interaction with the four ^{14}N nuclei.

4. Numerical simulations of DNP

4.1. Simulation methods

Once we have some information about the solid-state ESR lineshape and relaxation of the verdazyl-ribose radical, we can attempt to gain some insight into its DNP by numerical simulation of cross-

Table 3
ESR lineshape best fit parameters and results from quantum chemistry calculation. Note that the sign of the hyperfine couplings is not determined by the experiment. Error values are roughly estimated from the range of acceptable lineshape fits.

Parameter	Axis (relative to ring plane)	Best fit value	Quantum chemistry calculation
G-tensor	Perpendicular	2.0023 ± 0.0003	2.0021
	In plane	2.00445 ± 0.0003	2.0047
	In plane	2.00495 ± 0.0003	2.0051
^{14}N hyperfine couplings, MHz	Perpendicular	40 ± 4	38.0, 36.8
Nitrogen atoms A & B (bonded to carbonyl C)	In plane	2 ± 2	−1.2, −1.1
	In plane	2 ± 2	−1.0, −1.0
^{14}N hyperfine couplings, MHz	Perpendicular	53 ± 4	54.1, 51.5
Nitrogen atoms C & D	In plane	4.1 ± 2	−2.8, −3.1
	In plane	4.1 ± 2	−2.1, −2.4
Line broadening		12 (1.2 T)	
Gaussian FWHM, MHz		24 (9.4 T)	

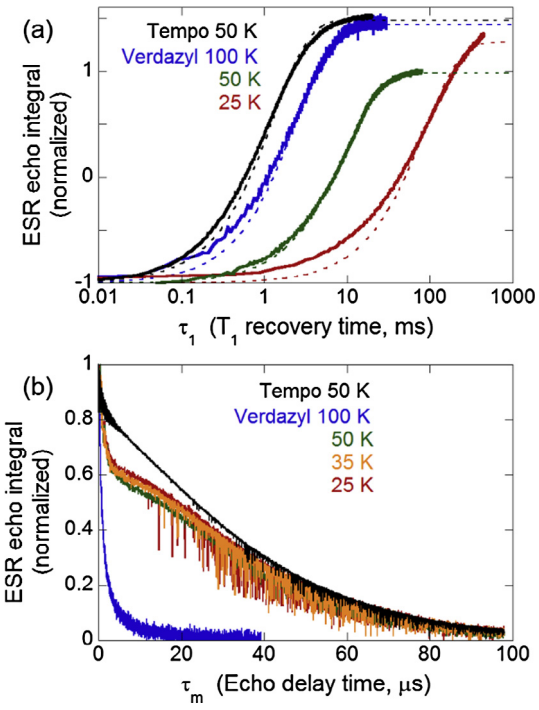

Fig. 5. 1.2 T (Q-band) ESR relaxation: (a) electron spin-lattice relaxation, T_{1e}, (b) phase memory relaxation time, T_m. These relaxation curves were measured at the maximum of the ESR lineshapes. The T_{1e} relaxation in part (a) is only roughly single exponential, but the fits are shown with dashed lines, and have time constants of 1.3 ms for TEMPO at 50 K, and 2.4, 9.9, and ~86 ms for verdazyl-ribose at 100, 50 and 25 K, respectively.

effect DNP with MAS. In this article, we choose to simulate hypothetical bi-radical molecules for several reasons, even though the experiments are done on solutions of mono-radicals. First, the cross-effect requires pairs of radicals, so the simulations must include the interaction between pairs of electron spins. Thus, a cross-effect DNP simulation of bi-radicals is not fundamentally different from a simulation of mono-radicals. If the radicals are randomly distributed in a frozen solution of mono-radicals, there will be a distribution of distances between neighboring electron spins. As a result, there will be a random distribution of clusters of interacting electron spins. As a concrete example, for a random distribution, over 30% of electron spins would be in a cluster of 5 or more interacting spins, even if only the nearest neighbor interaction of each electron spin is kept. While simulating these larger spin clusters should be possible, it is not clear that the added complexity and required averaging over the random clustering would pay off in greater understanding of the experiments. Therefore, we have chosen to simplify the simulations by using pairs of radicals separated by a fixed distance. Despite the simplifications in the simulations, we hope that they offer some insight into the relative DNP efficiency of the verdazyl radical. Beyond that, the second reason we are simulating bi-radicals is to predict whether synthesizing bi-radical molecules that include verdazyl radicals is likely to be a promising avenue for improved DNP. Previous work has shown that molecules containing multiple radicals can significantly improve cross-effect DNP, compared to mono-radicals [11,25,39,40]. To help predict the benefit of molecules containing verdazyl radicals, we simulate hypothetical molecules with two verdazyl radicals, and with one verdazyl and one nitroxide radical, and compare the simulated DNP to that from a bi-radical molecule with two nitroxides.

A third motivation for simulating the cross-effect DNP using a fixed distance between pairs of radicals is that we can use the method of numerical calculation already described in a previous paper [29]. For the full details, the reader should refer there, but we will sketch the general outline here. Cross-effect DNP relies on having two electron spins with a frequency difference between their ESR frequencies that equals the NMR frequency. When this is the case, the nuclear polarization can equilibrate toward the polarization difference between the two electron spins, through spin transitions that flip all three spins. Therefore, the basic unit of the model is a three-spin group (two electron and one nuclear spins) to represent a bi-radical molecule and one ^{1}H nucleus close to one of the electrons. Included in the simulation are the interactions of all three spins with the large static magnetic field, which determines two ESR frequencies (ω_{e1} & ω_{e2}), and one NMR frequency (ω_n). In addition, there is the dipole coupling between the two electrons, a hyperfine coupling between the nucleus and one of the electrons, and the microwave magnetic field at a frequency close to the ESR frequencies. Unless otherwise specified, the parameter values used in the simulations are given in Table 4. To include intermolecular electron spin diffusion, we use 1000 of these three-spin groups, thus each simulation has a total of 3000 spins.

In order to simulate this many spins conveniently, we do not use a full quantum mechanical calculation. As discussed previously [10], DNP under MAS can be viewed as a series of population transfers at spin energy level crossings. The ESR frequencies have a significant dependence on the molecular orientation relative to the magnetic field, due to anisotropy of the g-tensor and the ^{14}N hyperfine couplings. Thus the ESR frequencies vary as a function of the rotor orientation in MAS, causing crossings between the different energy levels. The NMR frequency has a much smaller orientation dependence, and the NMR frequency is taken as constant in these calculations. The dynamics of the full quantum mechanical system can be well approximated by using the analytical Landau-Zener formula [20,21] to calculate the probabilities of spin transitions during the level crossings. Three types of energy level crossings are important for cross-effect DNP: (i) Electron-microwave crossings, where an ESR frequency crosses the microwave frequency (ω_m), which can flip an electron spin; (ii) Three-spin crossings, where $\omega_{e1} - \omega_{e2} = \omega_n$, which can flip all three spins. Only three-spin crossings involving spins within the same biradical are included in these simulations; (iii) Electron-electron crossings, where two ESR frequencies are equal, which can produce a flip-flop transition of the two electrons. Electron-electron crossings involving electron pairs within the same biradical and electron pairs within different biradicals that are separated by less than 45 Å are included. Additionally, effects of T_{1e} relaxation are calculated by including partial population transfers toward a Boltzmann distribution at each time step as previously described [10]. T_2 relaxation is not necessary because the Landau-Zener formula does not create coherences between states.

Table 4
Standard values of parameters in simulations.

Parameter	Standard value
Microwave strength, $\omega_1/2\pi$	800 kHz
^{1}H NMR frequency, $\omega_n/2\pi$	−400.9 MHz
Temperature, T	25 K
MAS frequency, $\omega_r/2\pi$	7.0 kHz
Electron-electron coupling, $d_{max}/2\pi$	23 MHz
Hyperfine coupling, $h_{zz,max}/2\pi$	9 MHz
T_{1e} (verdazyl)	15 ms
T_{1e} (nitroxide)	2 ms
Bi-radical concentration	15 mM

The verdazyl T_{1e} is estimated by assuming that the ratio of verdazyl to nitroxide T_{1e} at 9.4 T is the same as measured at 1.2 T and 50 K. See Ref. [10] for justifications of the other parameter values.

With the simplified, analytical Landau-Zener dynamics, we can calculate the time dependences of spin polarizations for all 3000 spins as follows. First, the biradical orientations are chosen randomly. Each biradical orientation consists of random orientations of the electron g-tensors, electron-electron dipole-dipole coupling tensor, and electron-nucleus hyperfine coupling tensor principal axes in the MAS rotor. No correlations among the various orientation angles are used. The electron-^{14}N hyperfine couplings are included, with the ^{14}N spin states randomly chosen, and kept fixed during the calculations. (The electron-^{14}N hyperfine couplings effectively modify the electron g-tensor, but have no other effect.) The positions of the biradicals are chosen randomly in a cube sized to simulate the desired biradical concentration. These positions are used to calculate intermolecular electron-electron couplings. Configurations with electron-electron distances less than 2.5 Å are rejected.

The simulations begin with an equilibration period of $5T_{1e}$, without ^{1}H hyperfine coupling. This allows the electron spins to reach their equilibrium polarizations under MAS. Then, the ^{1}H hyperfine coupling is included, and the time dependence of the nuclear spin polarizations is calculated for 100 ms starting from two different initial conditions: (i) thermal equilibrium of the nuclear spins at 25 K; and (ii) the nuclear spins polarized to the thermal value for an electron spin. By considering two different initial conditions, we avoid the problem of distinguishing between a bi-radical orientation which has no net cross-effect relaxation and an orientation that happens to have a final steady-state nuclear spin polarization close to the initial nuclear spin polarization. These calculations result in two roughly exponential curves for the nuclear spin polarization in each three-spin system. Fitting the two curves together results in a common time constant and steady-state nuclear spin polarization. The values for the 1000 three-spin systems in each simulation are averaged together as in Eq. (1) to derive an average steady-state nuclear polarization, $p_{n,ave}$, and an average time constant for polarization of one close nucleus, $t_{\mathrm{DNP,ave}}$,

$$p_{n,ave} = \frac{\sum_{k=1}^{N}\left(\frac{p_n}{t_{\mathrm{DNP}}}\right)_k}{\sum_{k=1}^{N}\left(\frac{1}{t_{\mathrm{DNP}}}\right)_k} \tag{1a}$$

$$\frac{1}{t_{\mathrm{DNP,ave}}} = \frac{1}{N}\sum_{k=1}^{N}\left(\frac{1}{t_{\mathrm{DNP}}}\right)_k \tag{1b}$$

where the index k represents a single biradical orientation and N is the number of orientations.

4.2. Simulation results

Fig. 6 shows $p_{n,ave}$ and $t_{\mathrm{DNP,ave}}$ as a function of microwave frequency for three different possible bi-radical molecules: molecules with two verdazyl radicals, two nitroxide radicals, and a mixed bi-radical with one verdazyl and one nitroxide. The calculated frequency dependence for a verdazyl-verdazyl bi-radical has a positive peak in the nuclear polarization that is much larger than the negative peak. This arises from the asymmetric ESR lineshape, and is qualitatively consistent with the experimental results. The cross-effect DNP is largest when the microwave frequency is on the low-frequency tail of the ESR lineshape, roughly separated by the NMR frequency from the peak of the ESR lineshape. In contrast, having the microwave frequency at the peak of the ESR lineshape provides much smaller DNP. This probably results from an "oversaturation" regime, where the polarization of the entire ESR line is significantly reduced by the microwaves, thus reducing the polarization difference between electron spin pairs (see Suppl. Fig. S4). As a result, applying the microwaves to a region of the

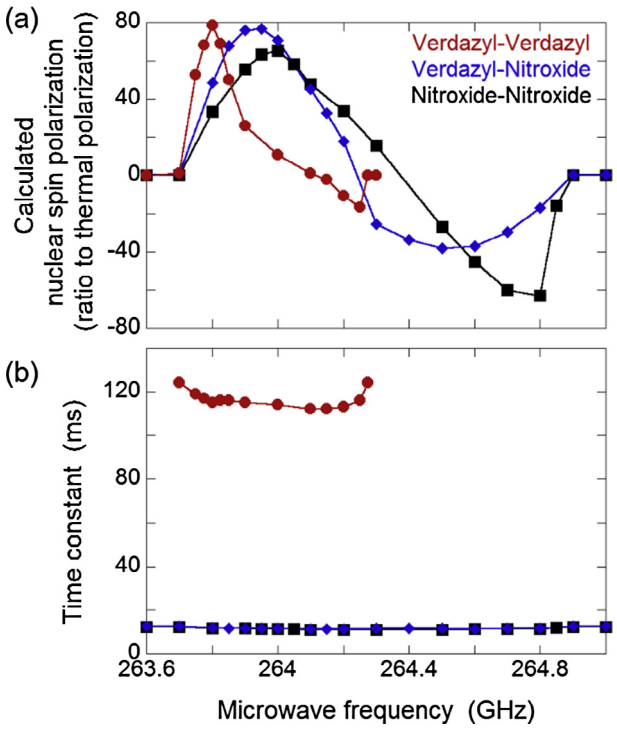

Fig. 6. (a) Calculated average nuclear spin polarization, $p_{n,ave}$, and (b) time constant, $t_{\mathrm{DNP,ave}}$, for verdazyl-verdazyl (red circles), verdazyl-nitroxide (blue diamonds), and nitroxide-nitroxide (black squares) bi-radicals. Parameters used are given in Table 4. Lines are drawn to guide the eye. (For interpretation of the references to colour in this figure legend, the reader is referred to the web version of this article.)

ESR line where there are relatively few spins is better, because it effectively reduces the microwave saturation. Another notable result of the simulations is that the average time constant is very long for the verdazyl-verdazyl bi-radical. The average time constant is long because only 4% of the bi-radicals have a three-spin energy level crossing. The average time constant thus ends up ~25× larger (1/0.04) than the typical time constant for polarization in a three-spin system with a three-spin energy level crossing. It is important to note that this is influenced by having fixed ^{14}N spin states in the simulations. If the ^{14}N spins are allowed to sample all possible states, 57% of randomly oriented verdazyl-verdazyl bi-radicals will have a three-spin energy level crossing. Therefore, we would expect additional averaging between cross-effect active and inactive states on a timescale determined by the ^{14}N T_1, that is not present in these simulations. We do not know what ^{14}N T_1 is in the verdazyl-ribose radical, or even for a nitroxide radical under our conditions of low temperature and high magnetic field [41]. So, we have chosen to fix the ^{14}N spin states (long ^{14}N T_1) to simplify the calculations, and to illustrate that the ^{14}N spin states help determine whether a verdazyl-verdazyl bi-radical is active for cross-effect DNP of ^{1}H at 9.4 T. If ^{14}N relaxation does occur on a short timescale, this should not affect the average results of the simulations. With fixed ^{14}N spin states, the simulations have a few verdazyl-verdazyl bi-radicals active for the cross-effect all the time, while with ^{14}N relaxation, more bi-radicals would be active, but only for part of the time. The overall average simulated DNP efficiency should remain constant.

These calculations suggest that the verdazyl radical has a linewidth at 9.4 T that is only barely wide enough for cross-effect DNP with two verdazyl radicals. Because the magnetic-field-independent ^{14}N hyperfine couplings make up a significant part of the electron linewidth even at 9.4 T, we would expect the verdazyl radical to work better at magnetic fields lower than 9.4 T,

because the ESR linewidth will be wider relative to the ^{1}H NMR frequency.

Comparing the calculations shown in Fig. 6 for the different bi-radicals, the peak nuclear polarization is very similar for all three types. The verdazyl-nitroxide bi-radical has a slightly higher peak average nuclear polarization than the nitroxide-nitroxide bi-radical, with a very similar polarization time constant. We should emphasize that part of the similarity of the calculated values results from using the same electron-electron dipole coupling, and hyperfine coupling for all bi-radical types. This enables a simple comparison because only the electron lineshapes and T_{1e} are changing. However, in actual bi-radicals, the spin-spin couplings will also be affected by the detailed geometrical differences between different types of bi-radicals. The average nuclear polarization and time constant of the verdazyl-nitroxide bi-radical is not strongly affected by the longer T_{1e} of the verdazyl radical. If the verdazyl T_{1e} is set equal to the nitroxide T_{1e} of 2 ms, the peak average nuclear polarization is 83× thermal polarization, and the time constant is 11.6 ms, nearly equal to the values of 77× and 11.6 ms calculated with the verdazyl T_{1e} equal to 15 ms. These calculations are in the regime where the long T_{1e} values are causing reduced nuclear polarization because of the near saturation of all of the electron spins. This can be seen in Fig. 7, where the calculated electron spin polarization is shown for a verdazyl-nitroxide bi-radical with microwave irradiation at 263.95 GHz. Even on the high frequency side of the nitroxide lineshape away from the microwave frequency, the electron spin polarization is only ~0.2 of the thermal polarization. With the minimum electron polarization at ~0, the polarization difference between the two electron spins of the bi-radical is ⩽0.2 of thermal polarization. Since the cross-effect DNP transfers this electron spin polarization difference to the nuclear spin polarization, the nuclear spin polarization cannot be very high in this case. If however, the T_{1e} values are set 10× shorter (1.5 ms for verdazyl, 0.2 ms for nitroxide), the peak average nuclear polarization is calculated as 260× thermal polarization, more than three times higher. In contrast, the polarization time constant of 11.4 ms does not change significantly with the change in T_{1e}.

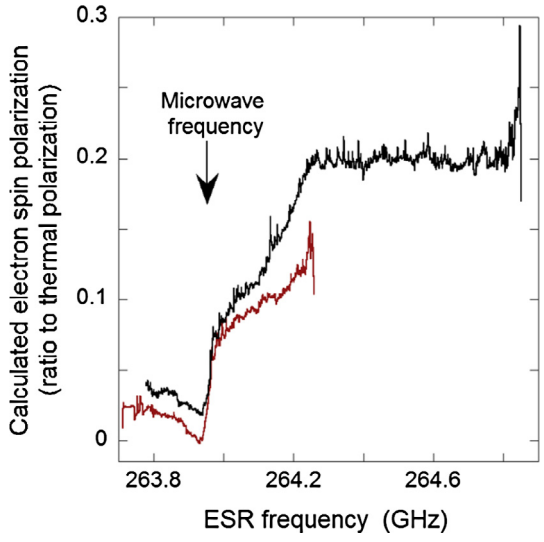

Fig. 7. Calculated electron spin polarization across the ESR lineshape for a verdazyl-nitroxide bi-radical. The verdazyl polarization is shown in red, and the nitroxide polarization in black. The microwave frequency is 263.95 GHz, and the other parameters are given in Table 4. (For interpretation of the references to colour in this figure legend, the reader is referred to the web version of this article.)

5. Discussion

These experiments demonstrate that the verdazyl-ribose radical can provide significant cross-effect DNP. Without MAS, the verdazyl-ribose radical provides larger DNP than the 4-hydroxy-TEMPO nitroxide. The ESR results suggest one possible reason. For the verdazyl radical, the maximum DNP occurs when the microwave frequency is on the low-frequency tail of the ESR lineshape. In that region of the ESR lineshape, the ESR frequency of an electron spin is significantly affected by its large ^{14}N hyperfine couplings. As a result, as the ^{14}N nuclear spin states change, a particular electron spin will move in and out of resonance with the microwave frequency. This may allow more electron spins to be saturated, and improve the DNP. This effect is similar to modulating the magnetic field or microwave frequency, which is known to have a beneficial effect for DNP with static samples [23]. Another possibility is that the narrower, axial ESR lineshape of the verdazyl is better for non-spinning DNP, compared to the broader, more symmetric line of the nitroxide.

However, the narrower ESR lineshape of the verdazyl-ribose is only marginally wide enough for cross-effect DNP. The verdazyl ESR line at 9.4 T is only slightly wider than the ^{1}H NMR frequency of 400 MHz. Because the spread of g-values alone is not enough to cover the NMR frequency, the verdazyl DNP is relying on the additional linewidth from the magnetic-field-independent hyperfine couplings. As a result, at lower magnetic field, the verdazyl ESR line will be wider relative to the NMR frequency. So, we would expect the verdazyl cross-effect DNP to work better at fields below 9.4 T for this reason, in addition to other magnetic field dependences of the cross-effect [10].

With MAS, at low temperatures (~30 K), and moderate microwave power (1.5 W), the verdazyl-ribose does not provide as much nuclear polarization as the nitroxide. In addition, the polarization buildup time is longer. There might be several reasons for this, such as longer T_{1e}, narrower ESR line, or weaker ^{1}H hyperfine couplings. The numerical simulations of DNP with MAS suggest that a major factor is that the ESR line is too narrow, leaving many verdazyl radical pairs without any three spin flip energy level crossings during the entire MAS rotation. When the microwave power is reduced or the temperature increased, the verdazyl radical DNP with MAS becomes comparable to the nitroxide. This is consistent with the longer T_{1e} of the verdazyl radical making it easier to saturate the electron spins at higher temperature or with lower microwave power.

In this article, we have primarily compared DNP results from two mono-radicals, to demonstrate the DNP efficiency of the verdazyl mono-radical, without including the additional factor of mono-radical versus multi-radical molecules. However, it is worth comparing the verdazyl results to multi-radical molecules. With MAS, multi-nitroxide dopants can provide higher signal enhancement and faster polarization buildup time than the verdazyl mono-radical. This is not surprising because the development of bi-nitroxide molecules was important for improving the efficiency of cross-effect DNP [11]. As a specific example, the tri-nitroxide molecule DOTOPA-ethanol can provide a DNP enhancement of 128 with a polarization buildup time of 3.8 s, at 25 K and 6.7 kHz MAS [24], for a similar sample in the same DNP setup as used for the experiments in this article. Without MAS, the mono-radical verdazyl has a more competitive DNP enhancement and polarization buildup time. For example, the 74× enhancement and 32 s buildup time at 29 K for verdazyl from Table 1 can be compared to a 47× enhancement and 14 s buildup time at 19 K for 10 mM tri-nitroxide DOTOPA-4OH from Ref. [29]. However, it should be noted that the most commonly used bi- [12] and tri-nitroxide molecules have generally been chosen for strong DNP under MAS

conditions, so they may not be optimal for non-spinning conditions. Overall, the verdazyl-ribose mono-radical is much less efficient than the best multi-nitroxide radicals under our DNP conditions with MAS, but is comparable in DNP efficiency without MAS.

Since cross-effect DNP requires two electron spins at different frequencies, the verdazyl-ribose radical could be used in combination with another type of radical. This strategy of using two different radicals has been successfully tested with a trityl and a nitroxide radical [42]. Our numerical simulations of DNP with MAS suggest that a verdazyl-nitroxide bi-radical would be slightly better than a nitroxide-nitroxide bi-radical, assuming the same spin-spin coupling constants. At this stage, we cannot say whether the coupling constants, the electron-electron dipole coupling and electron-^{1}H hyperfine coupling, would be either stronger or weaker in an actual verdazyl-nitroxide bi-radical.

The verdazyl-ribose radical is effective for cross-effect DNP under our conditions, but it may also be useful for other DNP applications. Because this radical provides its best DNP for a non-spinning sample, it might work well for dissolution DNP, where the conditions are typically a non-spinning sample at ~1.4 K [43]. However, the long T_{1e} at low temperatures may hinder the DNP, or require a secondary dopant to shorten T_{1e} [44]. In addition, the verdazyl-ribose radical may be useful for solution-state DNP at high magnetic fields. The verdazyl radical was earlier shown to be effective at solution state DNP at low magnetic fields, and the positive signal enhancement for ^{13}C indicates the dominance of the scalar (contact) DNP mechanism that may continue to be effective at high magnetic field [18,19]. Another possible application for verdazyl-ribose is under conditions where nitroxides are not sufficiently stable. For example, in vivo, nitroxides often have lifetimes of only a few minutes [45,46]. Verdazyl radicals potentially have broader application than the cross-effect DNP demonstrated in this article.

In these experiments, we have shown that verdazyl-ribose can be an effective water-soluble dopant for cross-effect DNP at high magnetic field, both with and without MAS. The verdazyl radical provides better DNP without MAS than a nitroxide radical, 4-hydroxy-TEMPO, used for comparison. With MAS, the verdazyl radical underperforms the nitroxide, at low temperatures and high microwave power, but is comparable if the temperature is increased or microwave power reduced. We have demonstrated DNP with verdazyl-ribose as a mono-radical, but these results also suggest that the verdazyl radical would be effective with two verdazyls in a bi-radical molecule, or in combination with another type of radical, such as a nitroxide. The verdazyl radical may also be useful for other DNP applications, such as dissolution DNP or high field solution-state DNP.

Acknowledgment

We would like to thank Thomas Schmidt and James Baber for assistance with the ESR measurements, and Rob Tycko for discussions of the work and manuscript. This work was supported by the Intramural Research Program of the National Institute of Diabetes and Digestive and Kidney Diseases, a component of the National Institutes of Health, and by grants from CSUPERB and the National Science Foundation (grant CHE-1058077). Numerical calculations used the high-performance computational capabilities of the Biowulf Linux cluster at the National Institutes of Health.

Appendix A. Supplementary material

Supplementary data associated with this article can be found, in the online version, at https://doi.org/10.1016/j.jmr.2018.02.016.

References

[1] A.V. Kessenikh, V.I. Lushchikov, A.A. Manenkov, Y.V. Taran, Proton polarization in irradiated polyethylenes, Soviet Phys.-Solid State 5 (1963) 321–329.
[2] C.T. Farrar, D.A. Hall, G.J. Gerfen, S.J. Inati, R.G. Griffin, Mechanism of dynamic nuclear polarization in high magnetic fields, J. Chem. Phys. 114 (2001) 4922–4933.
[3] A. Abragam, W.G. Proctor, Une Nouvelle Methode De Polarisation Dynamique Des Noyaux Atomiques Dans Les Solides, C. R. Hebdomadaires Seances Acad. Sci. 246 (1958) 2253–2256.
[4] E. Erb, J.L. Motchane, J. Uebersfeld, Effet De Polarisation Nucleaire Dans Les Liquides Et Les Gaz Adsorbes Sur Les Charbons, C. R. Hebdomadaires Seances Acad. Sci. 246 (1958) 2121–2123.
[5] N. Bloembergen, On the interaction of nuclear spins in a crystalline lattice, Physica 15 (1949) 386–426.
[6] J. Vanhouten, W.T. Wenckebach, N.J. Poulis, Study of thermal contact between nuclear Zeeman system and electron dipole-dipole interaction system, Physica B & C 92 (1977) 210–220.
[7] R.A. Wind, M.J. Duijvestijn, C. Vanderlugt, A. Manenschijn, J. Vriend, Applications of dynamic nuclear-polarization in C-13 NMR in solids, Prog. Nucl. Magn. Reson. Spectrosc. 17 (1985) 33–67.
[8] T.R. Carver, C.P. Slichter, Polarization of nuclear spins in metals, Phys. Rev. 92 (1953) 212–213.
[9] T.V. Can, M.A. Caporini, F. Mentink-Vigier, B. Corzilius, J.J. Walish, M. Rosay, W. E. Maas, M. Baldus, S. Vega, T.M. Swager, R.G. Griffin, Overhauser effects in insulating solids, J. Chem. Phys. 141 (2014).
[10] K.R. Thurber, R. Tycko, Theory for cross effect dynamic nuclear polarization under magic-angle spinning in solid state nuclear magnetic resonance: the importance of level crossings, J. Chem. Phys. 137 (2012).
[11] K.N. Hu, C. Song, H.H. Yu, T.M. Swager, R.G. Griffin, High-frequency dynamic nuclear polarization using biradicals: a multifrequency EPR lineshape analysis, J. Chem. Phys. 128 (2008).
[12] C. Sauvee, M. Rosay, G. Casano, F. Aussenac, R.T. Weber, O. Ouari, P. Tordo, Highly efficient, water-soluble polarizing agents for dynamic nuclear polarization at high frequency, Angew. Chem.-Int. Edit. 52 (2013) 10858–10861.
[13] A. Potapov, W.M. Yau, R. Ghirlando, K.R. Thurber, R. Tycko, Successive stages of amyloid-beta self-assembly characterized by solid-state nuclear magnetic resonance with dynamic nuclear polarization, J. Am. Chem. Soc. 137 (2015) 8294–8307.
[14] A. Potapov, W.M. Yau, R. Tycko, Dynamic nuclear polarization-enhanced C-13 NMR spectroscopy of static biological solids, J. Magn. Reson. 231 (2013) 5–14.
[15] T.N. Le, H. Grewal, V. Changoco, V. Truong, D.J.R. Brook, Water soluble, chiral, verdazyl radicals derived from aldoses, Tetrahedron 72 (2016) 6368–6374.
[16] R. Kuhn, H. Trischmann, Uber auffallend stabile n-haltige radikale, Angew. Chem.-Int. Edit. 75 (1963) 294.
[17] R. Kuhn, Verdazyls + related nitrogen-containing free radicals, Angew. Chem.-Int. Edit. 3 (1964) 762.
[18] J. Trommel, Molecular motions and collisions in organic free radical solutions as studied by dynamic nuclear polarization, in: Applied Physics, TU Delft, 1978.
[19] W. Mullerwarmuth, R. Vilhjalmsson, P.A.M. Gerlof, J. Smidt, J. Trommel, Intermolecular interactions of benzene and carbon-tetrachloride with selected free-radicals in solution as studied by C-13 and H-1 dynamic nuclear polarization, Mol. Phys. 31 (1976) 1055–1067.
[20] J.W. Zwanziger, S.P. Rucker, G.C. Chingas, Measuring the geometric component of the transition-probability in a 2-level system, Phys. Rev. A 43 (1991) 3232–3240.
[21] C. Zener, Non-adiabatic crossing of energy levels, Proc. Roy. Soc. London Ser. a-Contain. Papers Math. Phys. Charact. 137 (1932) 696–702.
[22] K.R. Thurber, A. Potapov, W.M. Yau, R. Tycko, Solid state nuclear magnetic resonance with magic-angle spinning and dynamic nuclear polarization below 25 K, J. Magn. Reson. 226 (2013) 100–106.
[23] K.R. Thurber, W.M. Yau, R. Tycko, Low-temperature dynamic nuclear polarization at 9.4 T with a 30 mW microwave source, J. Magn. Reson. 204 (2010) 303–313.
[24] K. Thurber, R. Tycko, Low-temperature dynamic nuclear polarization with helium-cooled samples and nitrogen-driven magic-angle spinning, J. Magn. Reson. 264 (2016) 99–106.
[25] W.M. Yau, K.R. Thurber, R. Tycko, Synthesis and evaluation of nitroxide-based oligoradicals for low-temperature dynamic nuclear polarization in solid state NMR, J. Magn. Reson. 244 (2014) 98–106.
[26] K.R. Thurber, R. Tycko, Measurement of sample temperatures under magic-angle spinning from the chemical shift and spin-lattice relaxation rate of Br-79 in KBr powder, J. Magn. Reson. 196 (2009) 84–87.
[27] A.E. Bennett, C.M. Rienstra, M. Auger, K.V. Lakshmi, R.G. Griffin, Heteronuclear decoupling in rotating solids, J. Chem. Phys. 103 (1995) 6951–6958.
[28] W. Snipes, J. Cupp, G. Cohn, A. Keith, Electron-spin resonance analysis of nitroxide spin label 2,2,6,6-tetramethylpiperidone-N-oxyl (tempone) in single-crystals of reduced tempone matrix, Biophys. J. 14 (1974) 20–32.
[29] K.R. Thurber, R. Tycko, Perturbation of nuclear spin polarizations in solid state NMR of nitroxide-doped samples by magic-angle spinning without microwaves, J. Chem. Phys. 140 (2014).
[30] Q.Z. Ni, E. Markhasin, T.V. Can, B. Corzilius, K.O. Tan, A.B. Barnes, E. Daviso, Y.C. Su, J. Herzfeld, R.G. Griffin, Peptide and protein dynamics and low-

temperature/DNP magic angle spinning NMR, J. Phys. Chem. B 121 (2017) 4997–5006.
[31] G.W.T.M.J. Frisch, H.B. Schlegel, G.E. Scuseria, J.R.C.M.A. Robb, G. Scalmani, V. Barone, B. Mennucci, H.N.G.A. Petersson, M. Caricato, X. Li, H.P. Hratchian, J.B. A.F. Izmaylov, G. Zheng, J.L. Sonnenberg, M. Hada, K.T.M. Ehara, R. Fukuda, J. Hasegawa, M. Ishida, T. Nakajima, O.K.Y. Honda, H. Nakai, T. Vreven, J.A. Montgomery Jr., F.O.J.E. Peralta, M. Bearpark, J.J. Heyd, E. Brothers, V.N.S.K.N. Kudin, T. Keith, R. Kobayashi, J. Normand, A.R.K. Raghavachari, J.C. Burant, S.S. Iyengar, J. Tomasi, N.R.M. Cossi, J.M. Millam, M. Klene, J.E. Knox, J.B. Cross, C.A. V. Bakken, J. Jaramillo, R. Gomperts, R.E. Stratmann, A.J.A.O. Yazyev, R. Cammi, C. Pomelli, J.W. Ochterski, K.M.R.L. Martin, V.G. Zakrzewski, G.A. Voth, J.J.D.P. Salvador, S. Dapprich, A.D. Daniels, J.B.F.O. Farkas, J.V. Ortiz, J. Cioslowski, D.J. Fox, Gaussian 09, Revision E.01, in: Gaussian, Inc., Wallingford CT, 2013.
[32] V. Barone, Recent Advances in Density Functional Methods, Part I, World Scientific Publ. Co., Singapore, 1996.
[33] P.H.H. Fischer, LCAO-MO calculations on verdazyls, Tetrahedron 23 (1967) 1939.
[34] V. Barone, A. Bencini, I. Ciofini, C. Daul, Structure and magnetic properties of oxoverdazyl radicals and biradicals by an integrated computational approach, J. Phys. Chem. A 103 (1999) 4275–4282.
[35] J. Barilone, F. Neese, M. van Gastel, Finding the reactive electron in paramagnetic systems: a critical evaluation of accuracies for EPR spectroscopy and density functional theory using 1,3,5-triphenyl verdazyl radical as a testcase, Appl. Magn. Reson. 46 (2015) 117–139.
[36] S. Stoll, A. Schweiger, EasySpin, a comprehensive software package for spectral simulation and analysis in EPR, J. Magn. Reson. 178 (2006) 42–55.
[37] K.M. Salikhov, S.A. Dzuba, A.M. Raitsimring, The theory of electron spin-echo signal decay resulting from dipole-dipole interactions between paramagnetic centers in solids, J. Magn. Reson. 42 (1981) 255–276.
[38] R. Dastvan, B.E. Bode, M.P.R. Karuppiah, A. Marko, S. Lyubenova, H. Schwalbe, T.F. Prisner, Optimization of transversal relaxation of nitroxides for pulsed electron-electron double resonance spectroscopy in phospholipid membranes, J. Phys. Chem. B 114 (2010) 13507–13516.
[39] G. Mathies, M.A. Caporini, V.K. Michaelis, Y.P. Liu, K.N. Hu, D. Mance, J.L. Zweier, M. Rosay, M. Baldus, R.G. Griffin, Efficient dynamic nuclear polarization at 800 MHz/527 GHz with trityl-nitroxide biradicals, Angew. Chem.-Int. Edit. 54 (2015) 11770–11774.
[40] F. Mentink-Vigier, G. Mathies, Y.P. Liu, A.L. Barra, M.A. Caporini, D. Lee, S. Hediger, R.G. Griffin, G. De Paepe, Efficient cross-effect dynamic nuclear polarization without depolarization in high-resolution MAS NMR, Chem. Sci. 8 (2017) 8150–8163.
[41] I. Kaminker, T.D. Wilson, M.G. Savelieff, Y. Hovav, H. Zimmermann, Y. Lu, D. Goldfarb, Correlating nuclear frequencies by two-dimensional ELDOR-detected NMR spectroscopy, J. Magn. Reson. 240 (2014) 77–89.
[42] K.N. Hu, V.S. Bajaj, M. Rosay, R.G. Griffin, High-frequency dynamic nuclear polarization using mixtures of TEMPO and trityl radicals, J. Chem. Phys. 126 (2007).
[43] J.H. Ardenkjaer-Larsen, B. Fridlund, A. Gram, G. Hansson, L. Hansson, M.H. Lerche, R. Servin, M. Thaning, K. Golman, Increase in signal-to-noise ratio of > 10,000 times in liquid-state NMR, Proc. Natl. Acad. Sci. U.S.A. 100 (2003) 10158–10163.
[44] J.H. Ardenkjaer-Larsen, S. Macholl, H. Johannesson, Dynamic nuclear polarization with trityls at 1.2 K, Appl. Magn. Reson. 34 (2008) 509–522.
[45] F. Hyodo, K. Matsumoto, A. Matsumoto, J.B. Mitchell, M.C. Krishna, Probing the intracellular redox status of tumors with magnetic resonance imaging and redox-sensitive contrast agents, Cancer Res. 66 (2006) 9921–9928.
[46] R.M. Davis, S. Matsumoto, M. Bernardo, A. Sowers, K.I. Matsumoto, M.C. Krishna, J.B. Mitchell, Magnetic resonance imaging of organic contrast agents in mice: capturing the whole-body redox landscape, Free Radic. Biol. Med. 50 (2011) 459–468.